International Journal of Multiphase Flow 113 (2019) 142–152

Contents lists available at ScienceDirect

International Journal of Multiphase Flow

journal homepage: www.elsevier.com/locate/ijmulflow

A fully analytical model for virtual mass force in mixture flows

Shiva P. Pudasaini

Institute of Geosciences and Meteorology, Geophysics Section, University of Bonn, Meckenheimer Allee 176, Bonn D-53115, Germany

ARTICLE INFO

Article history:
Received 2 October 2018
Revised 4 December 2018
Accepted 14 January 2019
Available online 16 January 2019

Keywords:
Multi-phase mixture flows
Dispersed particles
Dilute and dense flows
Added mass
Virtual mass force
Analytical model

ABSTRACT

Virtual mass force plays important role in the dynamics of the mixture mass flow composed of viscous fluid and the solid particles. Often in practice, calibrated numerical values of the virtual mass force are used to validate the simulation results but largely without any further physical basis. Such values are limited to some lower limit of the solid volume fraction. This has restricted its applicability both in small scale and in large scale natural flow simulations where the virtual mass force should be automatically determined and controlled by the mechanical parameters and the flow dynamical variables involved in the mass movements. This requires a full analytical description of the virtual mass force in application that covers the whole domain of particle concentration distribution, from the vanishing limit to any upper limit that is needed. Based on a two-phase general mixture mass flow model (Pudasaini, 2012), here, we present a first-ever, fully analytical, smooth and well bounded model for the virtual mass force that overcomes these deficiencies, and thus the model is more appropriate for application in real flow simulations. The novel virtual mass force is general, evolves automatically as a function of solid volume fraction, is much more realistic and covers the whole spectrum of the flow as governed by the physical parameters, mechanics and dynamics of the mixture flow, including the concentration distribution, material densities and the mass fluxes. So, the new virtual mass force presents the most advanced model that exists for mixture mass flows. The strikingly novel observation and understanding is that the virtual mass force is maximum somewhere between dilute to dense distribution of the solid particles, or the dispersed phase, but not at the maximum solid volume fraction.

1. Introduction

Simulating multi-phase mass flows is of great interest in earth, environmental and energy science and technology, including the nuclear reactors and powerplants (Dong, 1978; Brennen, 1982; Cook and Harlow, 1984; Kolev, 2007). Modeling interaction between liquid-gas, or liquid-particle requires interfacial models for momentum transfer at their interface (Drew, 1983; Ishii and Mishima, 1984; Kendoush, 2008; Mergili et al., 2017; 2018a; Bout et al., 2018). Simulation results show that for accelerated flows, the introduction of the virtual mass force significantly improves the results, indicating that this force is not negligible (No and Kazimi, 1981; 1985; Bournaski, 1992; Maliska and Paladino, 2006). Drag and virtual mass are two important hydrodynamic forces in mixture flows, or in naval architecture, that act at the particle (or, a solid body) -fluid interface as interfacial momentum exchange. Drag and virtual mass forces are the most important components of the interfacial momentum transfer. In many technical and applied problems, only the drag force is considered as the interfacial force. This force arises from the viscosity and pressure along the interface and is related to the local interfacial gradients. Usually, virtual mass force is considered as a second order effect when compared with drag. However, with the strong relative accelerations, the correct modeling of the virtual mass force is of fundamental importance in order to achieve accurate predictions of the flow variables, including pressure and velocity fields (Ishii, 1990; Kleinstreur, 2003; Maliska and Paladino, 2006).

In accelerated particle or bubbly flows, virtual mass plays important role in accurately predicting the flow dynamics of the multi-phase flows. Whenever acceleration acts on a fluid flow either by externally applied acceleration on the fluid or by internal acceleration of a body (or, particles) within the fluid, additional fluid force will be induced on the surface of the body or, the particle in contact with the fluid (Brennen, 1982). These fluid inertial forces can be of significant importance in many multi-phase flow problems (Mergili et al., 2017; 2018a; Bout et al., 2018; Kattel et al., 2018). Virtual mass (also known as added mass) is a common phenomenon that determines the necessary work done by the particle moving in the fluid to change the kinetic energy associated with the motion of the fluid. When a particle moves through a quiescent or relatively slowly moving liquid, some liquid mass is carried

E-mail address: pudasaini@geo.uni-bonn.de

https://doi.org/10.1016/j.ijmultiphaseflow.2019.01.005
0301-9322/

by the particle alongwith it. This portion of the liquid mass is supposed to attain the particle velocity. This results in a virtual increase in the particle mass, originating the concept of virtual mass in the mixture (Kleinstreur, 2003; Maliska and Paladino, 2006).

Formulation of the virtual mass force introduces a coefficient, $\mathcal{C}$, called the virtual mass force coefficient, which describes the fraction of displaced fluid that contributes to the effective mass of the particle (Cook and Harlow, 1984). In the two-phase motion of a particle (or, a bubble) through a liquid, the total effective mass of the particle consists of the mass of the particle itself plus a virtual mass that arises from the inertial properties of the liquid in the immediate vicinity of the particle. In a simple situation, if a single isolated particle is accelerated in a stationary fluid, its acceleration requires the fluid in its immediate neighborhood to accelerate. The accelerating fluid in return induces an added mass effect onto the particle (Dong, 1978). Under sufficiently small amplitudes of motion, the added mass phenomenon can be described in terms of an added mass coefficient, $\mathcal{C}$ = added mass of fluid/reference fluid mass. By definition, the virtual mass force is equal to the mass of liquid ($\rho_f V_s$, where ρ_f is the fluid density, and V_s is the particle volume) carried by the particle (or, bubble) $\mathcal{C}\rho_f V_s$, that already includes the virtual mass force coefficient $\mathcal{C}$ times a suitably defined relative acceleration between phases.

For particles moving in a liquid, the liquid mass carried by the particles is substantial as compared to the mass of the particles. So, this influences the momentum balances. Therefore, when solid particles flow in a liquid environment, a typical example being particle-viscous fluid debris mixture (Hutter et al., 1996; Rickenmann, 1999; Iverson and Denlinger, 2001; Mulder and Alexander., 2001; McDougall and Hungr, 2004; Takahashi, 2007; von Boetticher et al., 2016), the virtual mass must be considered in such a system (Dong, 1978; Maliska and Paladino, 2006; Khattri and Pudasaini, 2018). This indicates the importance of virtual mass force in particle-fluid mixture flow, like debris flow. Virtual mass force has been recently included in modeling debris and similar gravitational mixture mass flows by Pudasaini (2012), that has been applied in real events by Mergili et al. (2017, 2018a, 2018b); Bout et al. (2018), and complex flow-obstacle-interactions by Kattel et al. (2018).

The added mass phenomenon for single isolated particle has been extensively investigated experimentally and analytically, and rather well understood. However, determination of the virtual mass force for multiple particles and higher particle concentration is still challenging. Theoretical treatment has been quite successful using the potential theory (Dong, 1978; Thomas et al., 1983). The virtual mass for a single particle has been derived by Lamb (1952); Prandtl (1952) and Milne-Thomson (1968) for simple-shaped and slowly moving bubble through an unbounded, inviscid fluid. By introducing entrapped liquid by the bubble, Cook and Harlow (1984) formulated the dynamics of bubble, entrapped fluid and the bulk. Their approach commenced with a three field formulation representing the bulk liquid, the bubble, and the surrounding liquid associated with the virtual mass inertia. With suitable descriptions for the relationships among the three fields, their formulation reduces to the usual two-field equations but, with an explicit representation for the virtual mass terms.

The added mass coefficient (also called hydrodynamic mass coefficient) depends on the flow configuration, dynamics, and the geometry and number of particles in the flow, and thus can vary substantially (Dong, 1978). The virtual mass force may also depend on the particle or bubble shape (Bournaski, 1992). Similarly, virtual mass force increases for particles closer to the wall (Simcik et al., 2008). This indicates that at regions of higher solid particle concentration, or particle accumulation, virtual mass force increases with the solid volume fraction, α_s. Numerical values of the added mass coefficient can be relatively high (some times even higher than 5) (Dong, 1978; Biesheuvel and Spoelstra, 1989; Kolev, 2007; Simcik et al., 2008). Theoretically it has been shown that for increasing particle concentrations, the virtual mass coefficient increases (Dong, 1978; Simcik et al., 2008). As the solid (or, particle or, bubble) volume fraction tends to unity, i.e., $\alpha_s \to 1$, $\mathcal{C}$ appears to increase exponentially. Which, however, is not realistic. This is intuitively clear, because the induced kinetic energy of the fluid can not approach infinity as the solid volume fraction increases. The data also indicates that $\mathcal{C}$ can not always increase exponentially, or unboundedly (Dong, 1978).

Different constitutive equations and models are presented for the virtual mass force (Zuber, 1964; Biesheuvel and Spoelstra, 1989; Bournaski, 1992; Maxey and Riley, 1993; Kolev, 2007; Kendoush, 2008). However, the modeling of the virtual mass force is still a largely unsolved problem as there is no consensus on it. So, the main challenge that still remains is the construction of a suitable constitutive equation or, a model for the virtual mass coefficient, that covers the whole spectrum of the flow dynamics. As the convective derivative can be written in many different ways, several relative acceleration models are available for virtual mass force (Wallis, 1969; Lyczkowski et al., 1978; Drew, 1983; Pudasaini, 2012). A key question, however, is how to model the coefficient $\mathcal{C}$ in the most appropriate and general way. The virtual mass coefficient is determined for most cases such that satisfactory agreement can be obtained between the calculated and experimental results (Lahey et al., 1980; Cheng et al., 1983; Maliska and Paladino, 2006) or, that numerical calculation can be stabilized (No and Kazimi, 1981; Watanabe and Kukita, 1992). Furthermore, the virtual mass has a profound effect upon the mathematical characteristic. For this reason, No and Kazimi (1981, 1985) suggested a quantitative bound on the coefficient of the virtual mass terms in obtaining mathematical hyperbolicity and numerical stability.

However, the major concern here is the modeling of the virtual mass force coefficient. Already from the relatively lower solid fractions, particle interaction effects become important. The fluid mass carried by the particles increase with number of particles. This clearly implies that $\mathcal{C}$ should be a function of solid (or, fluid) fraction (Bournaski, 1992). Zuber (1964); van Wijngaarden (1976); Mokeyev (1977); Nigmatulin (1979); Rivero et al. (1991), and Maxey and Riley (1993), all obtained theoretical or empirical values of virtual mass coefficient that can be approximated to 0.5, correct to some order of α_s, but with different agreements on the order of approximation (Drew, 1983; Biesheuvel and Spoelstra, 1989; Bournaski, 1992). Although these models are mostly valid to relatively small to negligible solid volume fractions, from the structural point of view, virtual mass coefficients increase monotonically as a function of solid volume fraction in these models. There seems to be a type of consensus that as $\alpha_s \to 0$, $\mathcal{C} \to 0.5$. Otherwise, the existing models either do not include the whole range of the solid (or, bubble) fraction distribution, i.e., the mixture from dilute to dense, or these models tend to show singularity (Zuber, 1964; van Wijngaarden, 1976; Drew, 1983; Ishii and Mishima, 1984; Biesheuvel and Spoelstra, 1989; Sangani et al., 1991; Bournaski, 1992; Zhang and Prosperetti, 1994; Simcik et al., 2008; Pudasaini, 2012), because the basic models used therein is $\mathcal{C} = 0.5(1 + 2\alpha_s)/(1 - \alpha_s)$, or their derivatives, which become singular as $\alpha_s \to 1$. Similar singularities are also observed in other added mass coefficient theories (Dong, 1978).

The value $\mathcal{C} = 0.5$ has mostly been used in practice for different types of flows, both dilute and dense mixture of particles and fluid or bubble and fluid, which, however, is quite questionable. So, a virtual mass coefficient model that covers the whole distribution of the solid particle concentration is needed. Here, we present such a fully analytical model for virtual mass force in mixture flows consisting of viscous fluid and the solid particles that covers the entire domain of the solid volume fraction. The

model is sufficiently smooth and bounded, with its maximum lying somewhere between the dilute to dense limits of particles. Here, we are interested to develop and present a new model and its essence and highlight its application potential.

2. The new virtual mass force model

2.1. The analytical model

Let α_s and α_f $(=1-\alpha_s)$ be the solid and fluid volume fractions, u_s and u_f be the solid and fluid-phase velocities, and $\gamma = \rho_f/\rho_s$ be the ratio between the fluid and the solid material densities in the mixture mass flow with depth h, and $h_s = \alpha_s h$ and $h_f = \alpha_f h$ be the solid and fluid material depths, respectively. Note that for simplicity, here, the model will be developed based on the depth-averaged dynamical variables (u_s, u_f, α_s). However, analogous models can also be developed for the non-depth averaged full-dimensional dynamical variables. We begin the model derivation by considering the solid and fluid mass fluxes from the general two-phase mass flow model in Pudasaini (2012):

$$\alpha_s h\big(u_s - \gamma \mathcal{C}\big(u_f - u_s\big)\big) = m_s, \tag{1}$$

$$\alpha_f h\left(u_f + \frac{\alpha_s}{\alpha_f}\mathcal{C}\big(u_f - u_s\big)\right) = m_f, \tag{2}$$

where, m_s and m_f are the virtual mass force induced solid and fluid mass fluxes, respectively, and as defined earlier, $\mathcal{C}$ is the virtual mass force coefficient. Then, by solving these equations, the virtual mass force coefficient $\mathcal{C}$ is obtained as a new fully analytical, but simple model:

$$\mathcal{C} = \frac{\mathcal{N}_{vm} - 1}{\alpha_s/\alpha_f + \gamma}, \tag{3}$$

where the non-dimensional quantity $\mathcal{N}_{vm}$ is called the virtual mass number, and is given by $\mathcal{N}_{vm} = \dfrac{\big(m_f/h_f - m_s/h_s\big)}{\big(u_f - u_s\big)}$, which is the ratio of the relative velocities obtained from the virtual mass force enhanced relative mass fluxes and the relative velocities. As the virtual mass force enhances the kinetic energy of fluid, and reduces the kinetic energy of solid, we have $m_f/h_f \geq u_f$, and $m_s/h_s \leq u_s$. Equality holds for the vanishing virtual mass force effects, for which $\mathcal{N}_{vm} = 1$, and consequently, $\mathcal{C} = 0$. The virtual mass force coefficient is a positive quantity, whenever there is non-zero relative acceleration between the phases. Thus, the structure of the novel virtual mass number $\mathcal{N}_{vm}$ indicates that $\mathcal{N}_{vm}$ must be (at least) greater than unity but, depending on the magnitudes of m_f and m_s, it can be much larger than unity. A typical value of $\mathcal{N}_{vm}$ is 1.2, which will be explained later.

2.2. The structure

Next, we analyze the structure of the virtual mass force coefficient $\mathcal{C}$ given by (3) and explore its dynamics. First, we note that $\mathcal{C} > 0$, and $\mathcal{C} = 0$ only if there is no effect of virtual mass in the mass flux, i.e., $\mathcal{N}_{vm} = 1$. $\mathcal{C}$ is a dynamic quantity and evolves with the flow depth h, and/or the volume fraction, α_s. Thus, $\mathcal{C}$ in (3) simultaneously includes the dynamical and physical aspects of the mixture flow through the volume fraction ratio α_s/α_f, and the density ratio $\gamma = \rho_f/\rho_s$. As $\gamma \to 1$, i.e., as the particles in the mixture become neutrally buoyant (Pudasaini, 2011), $\mathcal{C}$ decreases. This is realistic because, as $\gamma \to 1$, particle and fluid tend to move together that ultimately reduces the relative acceleration between the phases, resulting in the reduced value of $\mathcal{C}$, which is fully compatible with the physics of mixture flows. As $\alpha_f \to 0$ (or, $\alpha_s \to 1$), $\mathcal{C} \to 0$. This is also realistic, because as there is no fluid, no kinetic energy of the fluid needs to be induced. So, the structure of $\mathcal{C}$ in (3) automatically eliminates the singularity, while singularity was produced by the limit as $\alpha_s \to 1$ in several previous considerations (see, e.g., Zuber, 1964; Drew, 1983; Ishii and Mishima, 1984; Biesheuvel and Spoelstra, 1989; Bournaski, 1992; Simcik et al., 2008; Pudasaini, 2012), as discussed in Section 1. For vanishing solid fraction, the denominator of $\mathcal{C}$ tends to γ. Then, as $\gamma \approx 0.4 = 1100/2700$ is typical in most natural debris flows (Mergili et al., 2017; 2018a), with the choice of value of $\mathcal{N}_{vm} \approx 1.2$, we obtain $\mathcal{C} \approx 0.5$, which is the typical value of the virtual mass force coefficient, often used in literature, especially when $\alpha_s \to 0$ (Zuber, 1964; Dong, 1978; Drew, 1983; Ishii and Mishima, 1984; Biesheuvel and Spoelstra, 1989; Bournaski, 1992; Simcik et al., 2008). Although the ratio $\mathcal{N}_{vm}$, of the two fundamentally different relative velocities, is not yet fully closed (described), by now, we have some better understanding on the structure and range of the virtual mass force coefficient, $\mathcal{C}$ in (3).

2.3. The functional relation

The most important aspect now is to determine a functional relation of the virtual mass number, $\mathcal{N}_{vm}$ with the solid volume fraction, α_s, i.e., $\mathcal{N}_{vm} = \mathcal{N}_{vm}(\alpha_s)$. From the inspection of the virtual mass force induced mass fluxes in (1) and (2), it is evident that $\mathcal{N}_{vm}$ is very closely related to α_s, most probably linearly or as a monotonically increasing function of α_s, because increasing solid concentration generally increases $\mathcal{N}_{vm}$ as particles motion induce more kinetic energy of the fluid, and thus its flux. This analysis suggests the following functional relation between $\mathcal{N}_{vm}$ and α_s:

$$\mathcal{N}_{vm} = \mathcal{N}^0_{vm}(\ell + \alpha_s^n), \tag{4}$$

where $\mathcal{N}^0_{vm}, \ell, n$ are some parameters, yet to be determined. So, the new virtual mass force model (3) takes the form:

$$\mathcal{C} = \frac{\mathcal{N}^0_{vm}(\ell + \alpha_s^n) - 1}{\alpha_s/\alpha_f + \gamma}. \tag{5}$$

The dilute and dense limits of (5) are $\mathcal{C} = \big(\mathcal{N}^0_{vm}\ell - 1\big)/\gamma$ and $\mathcal{C} = 0$, as $\alpha_s \to 0$ and $\alpha_s \to 1$, respectively. As justified below, physically most relevant values for the parameters $\mathcal{N}^0_{vm}$, ℓ and n can be: $\mathcal{N}^0_{vm} = 10$, $\ell = 0.12$ and $n = 1$ that provide the well calibrated value of $\mathcal{C} = 0.5$ at the vanishing solid fraction (dilute limit of the dispersed phase).

2.4. The virtual mass number

The structure of the virtual mass force enhanced mass fluxes in (1) and (2) indicates that generally, the fluid mass flux is enhanced and the solid mass flux is reduced with the increasing solid concentration, α_s. The discussion in the following section shows that $n = 1$ represents plausibly one of the best choices. For this choice $\mathcal{N}_{vm}$ increases linearly with α_s. However, other scenarios are also possible. For example, $n = 0.5$ indicates that $\mathcal{N}_{vm}$ first increases rapidly, then slowly with α_s, which is also reasonable. And, $n > 1$ shows completely different behavior. The magnitude of the virtual mass number $\mathcal{N}_{vm}$ depends on the parameters $\mathcal{N}^0_{vm}$ and ℓ. However, its form and dynamics is determined by the flux intensity, n. The effects of n on $\mathcal{N}_{vm}$ has been presented in Fig. 1 for different n values. A typical value of the virtual mass number is 1.2 (as $\alpha_s \to 0$), and depending on the flux parameter, n, this number increases linearly, or non-linearly, and quickly or slowly.

The constant ℓ, when set lower or zero values, represents a cut off of the lower limit of α_s (see, Section 3.2.3). Technically, for debris flows, this value could be set to zero, because for very small value of α_s, the debris material behaves as a single-phase mixture

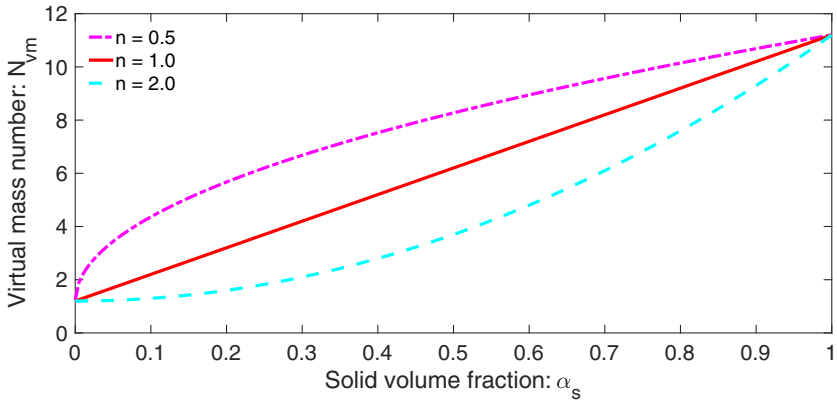

Fig. 1. The dynamics of the virtual mass number as the solid volume fraction evolves for the parameters $(\mathcal{N}^0_{vm}, \ell, \gamma) = (10, 0.12, 0.4)$, and different n values, $n = (0.5, 1.0, 2.0)$.

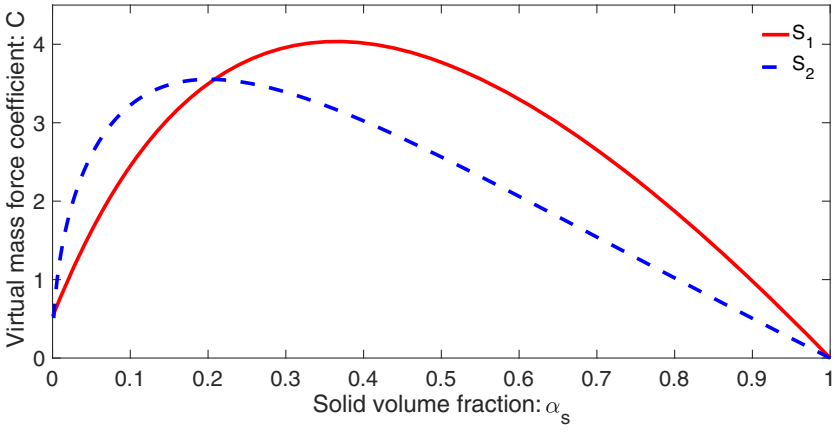

Fig. 2. The dynamics of the virtual mass force in mixture flow as the solid volume fraction evolves. The parameters are $S_1 : (\mathcal{N}^0_{vm}, \ell, n) = (10, 0.12, 1)$, and $S_2 : (\mathcal{N}^0_{vm}, \ell, n) = (5, 0.2, 0.5)$, respectively.

(Pudasaini and Hutter, 2007), typically a viscous fluid. In this situation, with $\ell \approx 0$, and $n = 1$, there is effectively a single parameter $\mathcal{N}^0_{vm}$, that adjusts the stretching and/or shifting of the virtual mass force coefficient $\mathcal{C}$. This reduces the number of parameters to one that can be fixed with the most often used or, calibrated values in the literature. Thus, in such a situation the new model is virtually free of fit parameters. This is often the most preferable choice in real applications (Bout et al., 2018; Mergili et al., 2018a; 2018b)

In most of the existing literature, the values of $\mathcal{C}$ are defined ad-hoc or, considered empirically (Zuber, 1964; Drew, 1983; Ishii and Mishima, 1984; van Wijngaarden, 1976; Sangani et al., 1991; Zhang and Prosperetti, 1994) with high accuracy up to α_s as large as 0.5 (Brennen, 2005). Based on the virtual mass force induced mass fluxes for solid and fluid in mixture flow, we have, for the first time, analytically derived a full mathematical expression for $\mathcal{C}$. In contrast to the existing models (Zuber, 1964; Jeffrey, 1973; van Wijngaarden, 1976; Mokeyev, 1977; Biesheuvel and Spoelstra, 1989) where only a certain local domain of the dispersed phase could be considered, the new model (5) covers the whole domain of the dispersed (solid) phase. The model is sufficiently smooth and physically well bounded with its maximum in between the dilute and dense limits of the solid fraction distribution, and evolves automatically as a function of changing solid volume fraction, including the physical parameters such as ratio between the fluid and solid densities, γ, and the flux intensity as incorporated by n in (5). Such a model is very suitable for complex mixture flow simulations (Mergili et al., 2017; 2018a; Bout et al., 2018; Kattel et al., 2018) rather than just a fixed parameter largely without any physical basis.

3. The full description and performance of the new model

3.1. The dynamics of the new virtual mass force model

In what follows, unless otherwise stated, and without loss of generality, we keep $\gamma = 0.4$ fixed, and consider two sets of parameters; $S_1 : (\mathcal{N}^0_{vm}, \ell, n) = (10, 0.12, 1)$, and $S_2 : (\mathcal{N}^0_{vm}, \ell, n) = (5, 0.2, 0.5)$. Fig. 2 reveals several dynamically interesting and mechanically important features of the virtual mass force (5) in mixture flow as the solid volume fraction evolves, covering the whole domain of α_s. Although validation with data is desirable, the parameter set S_1 may represent more realistic situation as the maximum of the virtual mass force for this set of parameters lies to the higher values of α_s than in the virtual mass force with parameter set S_2. The choice S_1 appears to be more supported by the existing literature (see, Fig. 4). Fig. 2 shows that the limiting values of the virtual mass forces for the two parameter sets are the same. However, their qualitative pictures and quantitative values both largely differ from each other.

3.1.1. The limiting values

The limiting value of $\mathcal{C} = 0.5$ as $\alpha_s \to 0$ is the most often used numerical value in literature (Zuber, 1964; van Wijngaarden, 1976; Drew, 1983; Ishii and Mishima, 1984; Sangani et al., 1991; Zhang and Prosperetti, 1994; Pudasaini, 2012; Mergili et al., 2017; 2018a; 2018b; Kattel et al., 2018) which is well captured by the new model.

On the one hand, reduction of $\mathcal{C}$ to its lower value (on the left) as α_s tends to vanish is justified as the effect of the enhanced fluid

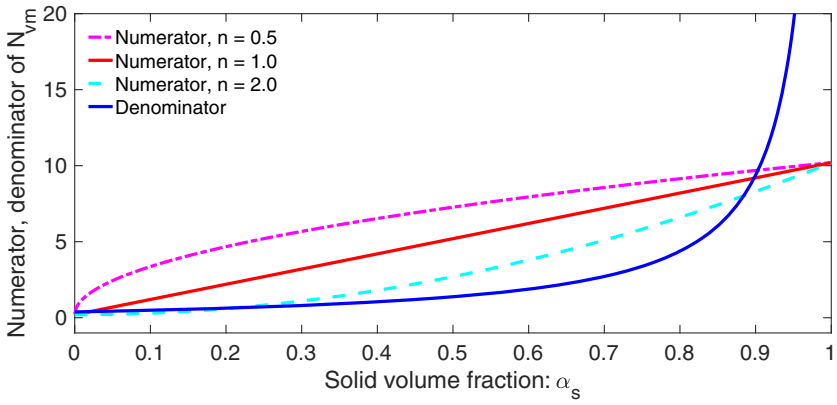

Fig. 3. Competition between numerator and denominator of $\mathcal{C}$ for different n values (0.5, 1.0, 2.0), keeping $(\mathcal{N}_{vm}^0, \ell, \gamma) = (10, 0.12, 0.4)$ fixed.

and reduced solid mass fluxes due to the virtual mass force reduces strongly with α_s tending to zero. On the other hand, $\mathcal{C} \to 0$ as $\alpha_s \to 1$ is governed by the vanishing enhancement of the relative mass fluxes (or, velocities). However, these mechanisms appear here automatically from the structure of the virtual mass force induced mass fluxes in Pudasaini (2012) as seen in (1) and (2), which is represented by the structure α_s/α_f in the denominator of $\mathcal{C}$.

3.1.2. Removal of singularity

Another very important observation is that the automatic appearance of γ (which is positive) and α_s/α_f in $1/(\alpha_s/\alpha_f + \gamma)$, or in the denominator of $\mathcal{C}$, removes singularity in the virtual mass force. As revealed by Fig. 2, this is a very important feature of the new full analytical model (5) for the virtual mass force.

3.1.3. The dry and fluid limits

As $\alpha_s \to 0$, there still exist some minimal effects of enhanced mass flux, so $\mathcal{C} > 0$. But, as $\alpha_s \to 1$, $\alpha_f \to 0$. So, there is almost no fluid whose kinetic energy needs to be enhanced because the mixture now behaves as if it was effectively dry, and thus the fluid related interfacial momentum transfer should vanish. Then, the debris flow turns into a dry avalanche, and thus $\mathcal{C} \to 0$. This is exactly represented by α_s/α_f in the denominator of $\mathcal{C}$. For $\alpha_s \to 1$, the solid is so packed that this cannot mobilize fluid to induce kinetic energy (even though there might still be some little amount of fluid). But, as $\alpha_s \to 0$, even very small amount of particles can still induce the kinetic energy of the surrounding fluid (Zuber, 1964; No and Kazimi, 1981; 1985; Drew, 1983; Ishii and Mishima, 1984; Biesheuvel and Spoelstra, 1989; Bournaski, 1992; Pudasaini, 2012). These characteristics of the virtual mass force are clearly observed in all the results presented here, in this and the following Sections.

3.1.4. Competition between numerator and denominator of $\mathcal{C}$

The dynamics and magnitudes of the numerator and denominator of $\mathcal{C}$ determine its form and values in Fig. 2, and other subsequent figures. As the form of $\mathcal{C}$ is largely determined by n, we consider different n values (0.5, 1.0, 2.0), keeping $(\mathcal{N}_{vm}^0, \ell, \gamma) = (10, 0.12, 0.4)$ fixed as before, and analyze how the numerator and denominator of $\mathcal{C}$ evolve (Fig. 3), and thus, how the dynamics of $\mathcal{C}$ is controlled.

For $n = 1$, denominator dominates the numerator for very small values of the solid volume fraction, $\alpha_s \leq 0.02$. Then, in the dilute regime (say, $\alpha_s \leq 0.4$) numerator increases steadily but, the denominator rises very slowly, whereas for $\alpha_s > 0.4$, the denominator increases, first rapidly, then exponentially as $\alpha_s \to 1$. They meet at about $\alpha_s = 0.89$ with values of numerator and denominator equal to 9.1, resulting in $\mathcal{C} = 1$. For $\alpha_s > 0.89$, as denominator increases exponentially, $\mathcal{C}$ drops to 0. Since only the numerator is n dependent, for other n values we only need to discuss how numerator evolves.

For $n = 0.5$, numerator increases rapidly in the very dilute regime ($\alpha_s \leq 0.1$), then it increases relatively slowly. Until $\alpha_s \leq 0.90$ numerator dominates denominator. But, for $\alpha_s > 0.90$ denominator strongly dominates numerator, that ultimately brings $\mathcal{C}$ to 0.

For $n = 2.0$, numerator increases very slowly in the limiting fluid regime ($\alpha_s \leq 0.2$). Then, the numerator increases quickly (quadratically) and meets the denominator already in the dilute regime at about $\alpha_s = 0.22$. Afterwards, numerator dominates denominator until $\alpha_s \approx 0.88$. Then, denominator strongly overtakes numerator, bringing $\mathcal{C}$ quickly down to 0.

In general, with the increasing α_s values from 0 to 1, denominator is larger, then smaller, and then larger again than the numerator, but these dominances are fundamentally different for different n values. Furthermore, it appears that the competition between the numerator and denominator of $\mathcal{C}$ for $n > 1.0$ (e.g., $n = 2$) appear to be more complex, resulting probably to a completely different flow dynamics (see, Figs. 6 and 11). This indicates the importance of the flux intensity.

3.1.5. The form of the virtual mass force coefficient

It is important to note how the form of $\mathcal{C}$ is developed in Fig. 2 as a result of the competition between the numerator and denominator of $\mathcal{C}$ discussed in Section 3.1.4, Fig. 3. The numerator of $\mathcal{C}$ increases steadily, whereas the denominator increases first very slowly, then slowly, then rapidly, and finally exponentially with α_s. For very small to small values of α_s, denominator dominates numerator. But, for small to larger α_s values, the numerator dominates. However, for very large values of α_s, the denominator strongly dominates the numerator due to the presence of α_s/α_f. This competition eventually controls the form of $\mathcal{C}$. In fact, the term α_s/α_f plays the great role in bringing $\mathcal{C}$ eventually down to zero after it attains maximum at certain value of α_s.

3.1.6. Recovering the existing models

The value of $\mathcal{C}$ as high as 5 (or, higher) are observed in literature even for the relatively low solid fraction $\alpha_s = 0.2$ (Dong, 1978; Biesheuvel and Spoelstra, 1989; Kolev, 2007; Simcik et al., 2008). Similarly, different virtual mass models show that $\mathcal{C}$ can be as high as 3.5, or even higher (Ishii and Mishima, 1984; Ishii and Hibiki, 2011). This has been shown in Fig. 4 with the new model.

The above discussion reveals that our analytical model extends the existing models and range of values of the virtual mass force by covering the whole domain of the distribution of the dispersive phase, while removing the singularity often seen in previous models.

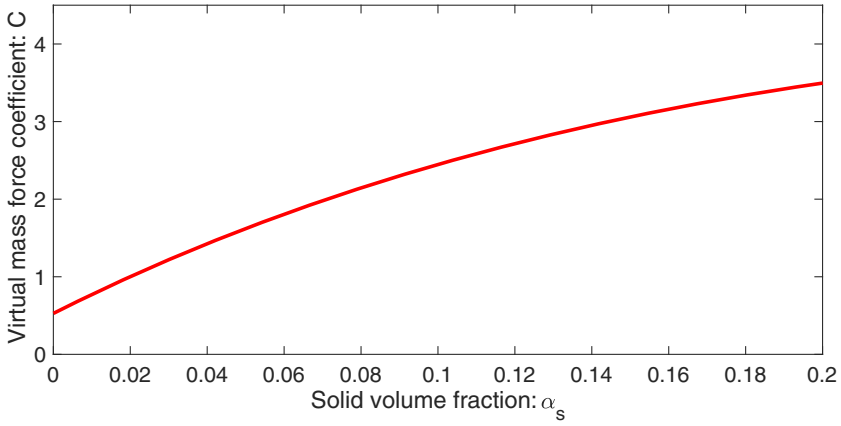

Fig. 4. Derived from Fig. 2. The detailed picture of the virtual mass force for more dilute-type flows with the lower values of the solid volume fraction.

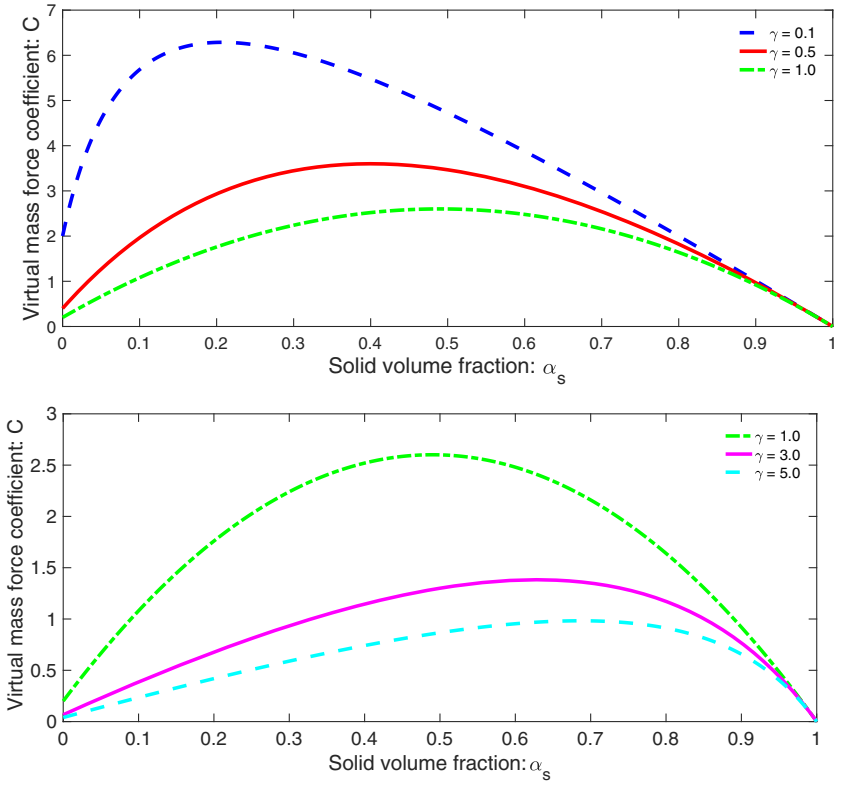

Fig. 5. Influence of material densities ($\gamma = \rho_f/\rho_f$) in virtual mass force.

3.2. Dynamics associated with different parameters

Next, we analyze in detail on how the range of parameters appearing in (5), namely, $\mathcal{N}_{vm}^0, \ell, n, \gamma$, influence the virtual mass force coefficient $\mathcal{C}$. For this, we expand the parameters in S_1 from Section 3.1, such that the previously chosen values are the representative values. One might think of linear effects of some of these parameters. However, the results below show highly non-linear dependency of $\mathcal{C}$ on all of these parameters. This discussion will show that, in general, proper modeling and choice of the parameters is important.

3.2.1. Influence of material densities

Since the material densities contained in γ, and the enhanced flux intensity described by n, fundamentally determine the form and magnitude of $\mathcal{C}$, first we analyze how these parameters play their role.

We begin by considering the effect of the densities in the mixture. Fig. 5 displays the effect of γ, which shows fundamental changes in the virtual mass force with the density ratio. Other material parameters are as in S_1. The value of γ less than unity corresponds to the heavier particles than the fluid, whereas the value of γ larger than unity correspond to the lighter particles than the fluid, and $\gamma = 1$ is the situation of the neutrally buoyant mixture (Bagnold, 1954; Pudasaini, 2011). The figure shows that as γ increases, the virtual mass force decreases rapidly, and at the same time the peaks shift quickly to the right (towards higher α_s values). However, for the neutrally buoyant flow ($\gamma = 1$), the peak of the virtual mass force lies close to the 50% of the particle concentration. This is quite reasonable, because it shows the balancing behavior of $\mathcal{C}$ both with solid fraction, and the densities. The impor-

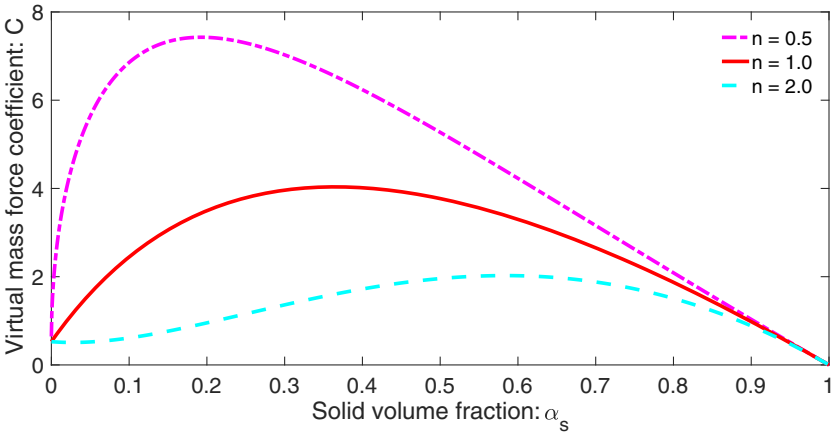

Fig. 6. Influence of mass flux in virtual mass force.

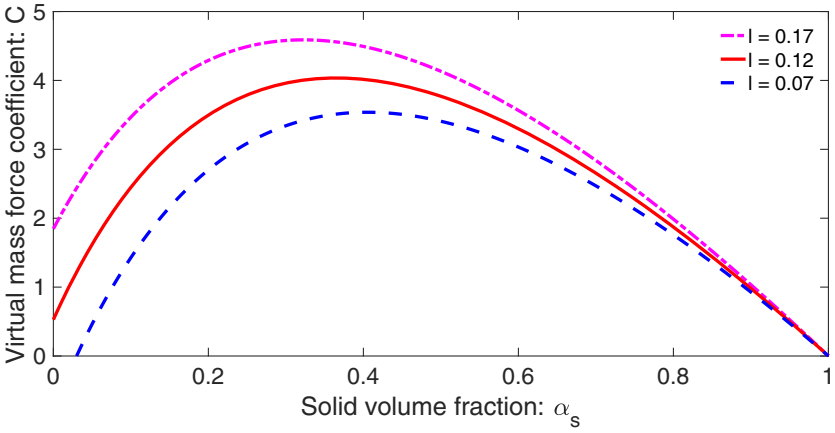

Fig. 7. Influence of the parameter ℓ in virtual mass force.

tant aspect here is that, with the appropriate choice of the parameters $\mathcal{N}_{vm}^0, \ell, n$, the new virtual mass force model (5) can potentially be applied for any type of mixture consisting of the fluid-solid and fluid-bubble with corresponding $\gamma < 1$, and $\gamma > 1$. The case $\gamma > 1$ is equally valid for woody debris flows (Shields and Gippe, 1995; Abbe and Montgomery, 1996) and the mixture flow where the rock particles like pumice stone (Ikeya, 1989; Crosta and Negro, 2003), whose density is fairly smaller than the viscous water. Fluid here refers to liquid or gas, that largely changes the γ values.

3.2.2. Influence of the enhanced flux

Fig. 6 shows the effects of the enhanced fluxes in virtual mass force associated with the parameter n. The lower value of n corresponds to the fast increase of the mass flux that later saturates with increasing α_s, whereas the higher values of n correspond first to the slow increase of the flux, that later increases rapidly for the higher solid fraction. The magnitude of the virtual mass force increases or decreases accordingly. Similarly, with the increasing value of n the peak of the virtual mass decreases and shifts to the domain of higher values of α_s. Also the geometric shapes of the $\mathcal{C}$ curves with changing n values are substantially to completely different both in quantity and quality. As explained in Section 3.1.4 , this is due to the different associated fluxes as described with n, and the competition between the numerator and denominator of $\mathcal{C}$. These results are compatible with the enhanced mass flux because it is directly related to the virtual mass force. Furthermore, we will see in Section 5, that the form of $\mathcal{C}$ with higher values of $n(>1)$ might better describe the virtual mass force for the motion of bubble-fluid mixture.

3.2.3. The parameter ℓ

Variation of $\mathcal{C}$ as a function of ℓ is presented in Fig. 7. The figure shows that the value of ℓ larger than 0.12 largely overestimates the reference curve (with $\ell = 0.12$), whereas the value of ℓ smaller than 0.12 underestimates the reference curve of $\mathcal{C}$ for the smaller values of the solid volume fraction, α_s. However, as α_s approaches its dry limit, all three curves meet each-other.

3.2.4. The parameter $\mathcal{N}_{vm}^0$

We further analyze the influence of the parameter $\mathcal{N}_{vm}^0$. The results are shown in Fig. 8. As compared to the results with variation in ℓ, now the virtual mass force coefficient deviates much more than in Fig. 7 from the reference curve associated with $\mathcal{N}_{vm}^0 = 10$. However, analogous to Fig. 7, larger value of $\mathcal{N}_{vm}^0$ than the reference value overestimates the reference curve and smaller value of $\mathcal{N}_{vm}^0$ underestimates the reference curve almost everywhere. A typical situation is that, the deviation is highest closer to the middle value of the solid volume fraction, α_s, whereas in Fig. 7 the largest difference was closer to the dilute limit (i.e., $\alpha_s \to 0$).

3.2.5. Parameter groups

The structure of $\mathcal{C}$ in (5), and the results presented so far, suggest organizing the parameters in two groups of different characteristics: $\mathcal{G}_1 = (n, \gamma)$, and $\mathcal{G}_2 = (\mathcal{N}_{vm}^0, \ell)$, determining the quality and magnitude of the virtual mass force coefficient. With the increasing (or, decreasing) values of $\mathcal{G}_1$, $\mathcal{C}$ decreases (or, increases). While, as the values of $\mathcal{G}_2$ increase (or, decrease), $\mathcal{C}$ increases (decreases). Although they play important role in determining the magnitude of $\mathcal{C}$, $\mathcal{G}_2$ could be structurally less important than

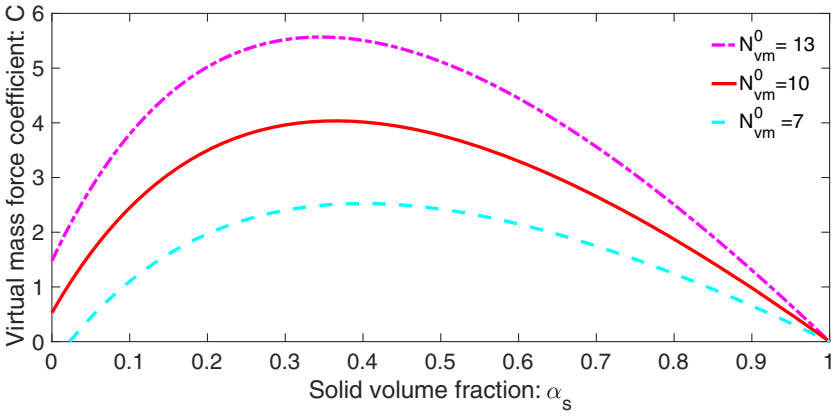

Fig. 8. Influence of the parameter $\mathcal{N}^0_{vm}$ in virtual mass force.

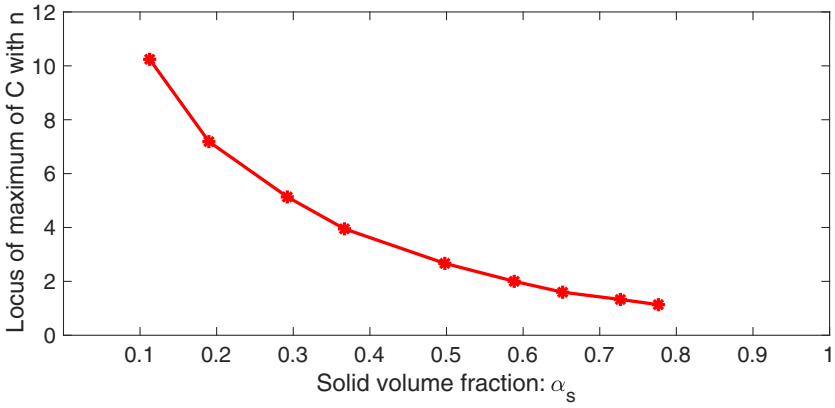

Fig. 9. The locus of the maximum of $\mathcal{C}$ as a function of α_s for different flux intensities n. The n values increase from left to right markers.

$\mathcal{G}_1$. Further, even more important point is that, $\mathcal{G}_1$ is associated with the material composition (thus the physics, included in γ) and flux (thus the dynamics, described by n). The parameter γ represents different material compositions. For solid particles-fluid mixture, γ is much lower than the same for the bubble-fluid mixture. Fig. 5 shows that for heavier dispersive phase (lower γ), the virtual mass force coefficient is higher and positively skewed, whereas this coefficient is lower and negatively skewed for the lighter dispersive phase (higher γ). Similarly, Fig. 6 displays higher and positively skewed $\mathcal{C}$ function for lower n value, and lower and negatively skewed $\mathcal{C}$ function for higher n value. These parameter studies clearly indicate that the proper choice of the parameters is necessary for the better simulation of the mixture mass flow associated with the virtual mass force.

3.3. Further properties of $\mathcal{C}$

3.3.1. Invariance of $\mathcal{C}$

Fig. 6 indicates the invariances of the limiting values of the virtual mass force coefficient $\mathcal{C}$. For any choice of the parameters $\mathcal{N}^0_{vm}, \ell, \gamma$ and n, $\mathcal{C}$ remains unchanged at $\alpha_s = 1$, i.e., $\mathcal{C}(1) = 0$. This is the dry limit of the mixture, where essentially there is no fluid, and thus the $\mathcal{C}$ values remain zero for any choice of the values of the physical parameters. However, for any suitably chosen values of $\mathcal{N}^0_{vm}, \ell, \gamma$, e.g., S_1 in Section 3.1, $\mathcal{C}$ remains invariant at the fluid limit ($\alpha_s = 0$) for any values of mass flux parameter n. In other words, $\mathcal{C}(0) = 0.5$. The structure of $\mathcal{C}$ in (5) indicates that, such invariance of $\mathcal{C}$ is only achievable for n values, and not for other parameters. That is, $\mathcal{C}(0) = 0.5$, and $\mathcal{C}(1) = 0.0$ are invariants for any n values, for a given proper set of $\mathcal{N}^0_{vm}, \ell$, and γ.

3.3.2. The locus of the maximum of $\mathcal{C}$

Another important observation of Fig. 6 is the locus of maxima of $\mathcal{C}$ with changing values of n. For small n values (e.g., 0.5), $\mathcal{C}$ attains its maximum of about 7.5 at about $\alpha_s = 0.175$. By increasing n just to 1.0, the maximum of $\mathcal{C}$ dramatically drops to about 4.0 and shifts substantially to $\alpha_s = 0.35$. Further increase of n to 2.0, results in a relatively small decrease of the maximum of $\mathcal{C}$ to about 2.0, but its maximum position has now been shifted much to the right at about $\alpha_s = 0.6$. The non-linear locus of $\mathcal{C}$ for different n values, $n = [0.3, 0.5, 0.75, 1.0, 1.5, 2.0, 2.5, 3.0, 3.5]$ is shown in Fig. 9. Furthermore, as discussed in Section 3.2.2, with respect to any reference value, e.g., $\mathcal{C} = 0.5$, the locus of the maximum values of $\mathcal{C}$ is relevant only for different n values. This is clear from the structure of $\mathcal{C}$ as $\mathcal{C}(0) = 0.5$ for any n values. Other parameter variation does not posses this property.

So, the parameter n associated with the mass flux plays an important role in determining the quality and quantity of the virtual mass force.

4. Enhanced virtual mass

The main essence of the virtual mass force is the added mass or the virtual mass. Here, we analyze a scenario to highlight how the new virtual mass force coefficient (5) enhances the mass by the added mass. For this, we consider the solid mass flux enhanced by the virtual mass from (1):

$$E_{M_f} = \rho_f \alpha_s h \, \mathcal{C}\big(u_s - u_f\big), \tag{6}$$

where γ is replaced by the relevant fluid density ρ_f to achieve the proper dimensional form, and the virtual mass force coefficient $\mathcal{C}$ is either 0.5 (the classical value), or given by the enhanced

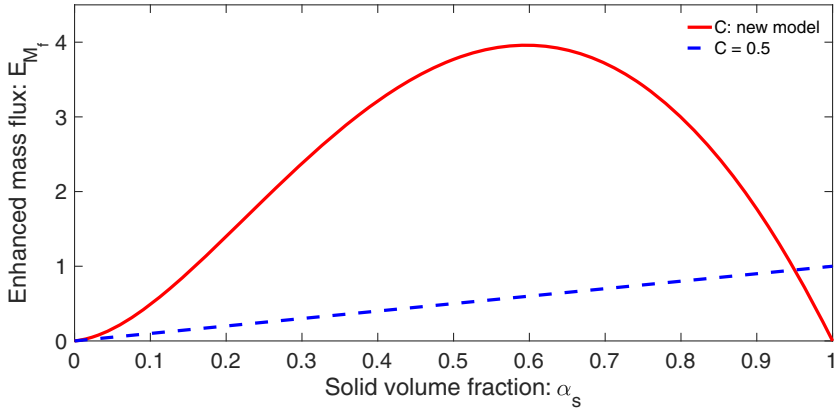

Fig. 10. Enhanced mass flux: Comparison between the classical and new added mass per unit time, normalized with fluid density ρ_f with the enhanced dynamical virtual mass force coefficient $\mathcal{C}$.

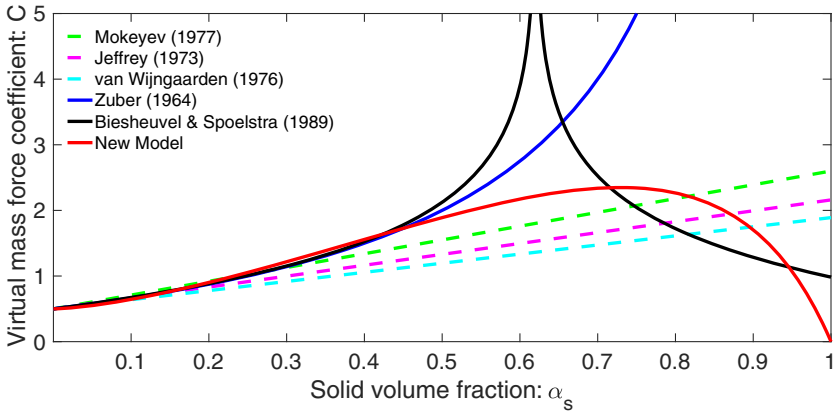

Fig. 11. Comparison between some classical virtual mass force coefficients, and the new virtual mass force coefficient $\mathcal{C}$, revealing the smooth and entire dynamics of the new model.

new model, (5). For simplicity, we consider some typical values of the parameters and variables at a given time: flow depth, $h = 2$ m; fluid density $\rho_f = 1100$ Kg m^{-3}; and the solid and fluid velocities are $u_s = 11$ ms^{-1} and $u_f = 10$ ms^{-1}, respectively (Mergili et al., 2017; 2018a; 2018b). So, momentarily, the relative velocity is about 1 ms^{-1}. The enhanced mass fluxes (E_{M_f}) given by (6) are shown in Fig. 10. For constant $\mathcal{C}$, E_{M_f} increases linearly with the solid volume fraction, α_s, indicating that the mass flux increases continuously with α_s and attains the maximum value at the solid limit, $\alpha_s = 1$. For the reasons given below, this, however, cannot be realistic. When the new analytical model for the virtual mass force coefficient $\mathcal{C}$ given by (5) is applied to (6), the situation is completely different. Although, quantitatively E_{M_f} also depends on other physical parameters (e.g., ρ_f) and dynamical variables (α_s, h, u_s, u_f), qualitatively it is fundamentally controlled by $\mathcal{C}$. This is clear from the shape of E_{M_f}, which is zero in the fluid ($\alpha_s \to 0$) and dry ($\alpha_s \to 1$) limits. As α_s increases from its left limit to higher values, E_{M_f} increases rapidly. Then, it attains its maximum value close to $\alpha_s = 0.6$, a typical value for dense packing. Then, for further higher values of α_s, the enhancement of the mass flux drops quickly, and becomes zero as α_s tends to unity. As discussed in Section 3.1, this behavior of the enhanced mass flux is realistic. So, the new model can better describe the dynamics associated with the virtual mass force in the mixture flow. Furthermore, the difference between the two enhanced mass fluxes with the most often used constant classical value of 0.5, and the new dynamical model of $\mathcal{C}$, is huge almost everywhere in the domain of the solid volume fraction. However, due to the presence of α_s in (6), the enhanced mass flux E_{M_f} behaves fundamentally differently than the virtual mass force coefficient $\mathcal{C}$ (Fig. 2), mainly for the dilute flows (i.e., $\alpha_s < 0.5$). So, it might be more relevant to talk about the virtual mass flux than the virtual mass force coefficient.

5. Comparison of the new model $\mathcal{C}$ with classical models

A direct comparison of the new virtual mass coefficient $\mathcal{C}$ with some extensively used existing models sheds further light on the importance of the new model. For this reason, we consider the models by Zuber (1964); Jeffrey (1973); van Wijngaarden (1976); Mokeyev (1977), and Biesheuvel and Spoelstra (1989) which are largely valid in dilute regimes, and the new model (5), which is valid for any mixture composition. Previous models are mainly based on the solid volume fraction α_s, but the new model includes further physics of the mixture and dynamics of the flow which makes it physically more appropriate and flexible. However, those models were mainly developed for fluid-bubble flows for which the physical parameters are different than those discussed in Sections 3 and 4. For example, in the fluid-bubble mixture, the density ratio γ is completely different than the one for solid particle-fluid (or, liquid) mixture representing a debris flow. So, we legitimately consider the parameters as: $\mathcal{N}_{vm}^0 = 25$, $\ell = 0.14$, $n = 1.5$, and $\gamma = 5$. The results are presented in Fig. 11, which reveal that the new model captures very well the dynamics of the other existing models in dispersive dilute regime, while the new model also removes the un-physical singularities and steadily increasing values of the virtual mass force in the relatively dense to dense regime of the dispersive phase. So, this proves the superiority and

application potential of the new model in the wide range of mass flows, and for any concentration of the dispersive phase.

As discussed in Section 3.2.5, the form of $\mathcal{C}$ is mainly determined by n and γ. The form and values of $\mathcal{C}$ in Fig. 11 can be justified. With respect to the same background fluid, consider two situations, one with the dispersive solid phase, and the other bubble phase. Then, the density ratio γ associated with the solid particles is much smaller than the same with the bubbles. Virtual mass induced flux in bubble-fluid mixture is less than virtual mass induced flux in debris mixture flows with dispersed solid particles. This is represented with the higher n values for bubble-fluid mixture. Increased n values eventually lower $\mathcal{C}$ in dilute regimes and uplift $\mathcal{C}$ in dense regimes. But, in magnitude, the $\mathcal{C}$ value, in general, is lower for the bubble-fluid mixture than the same for the solid particles-fluid debris mixture. This results in much higher virtual mass force for the solid particles-fluid mixture than in bubble-fluid mixture. So, the results in Figs. 2 and 11 are in line with this fact that the virtual mass force can be more pronounced in debris flows than in fluid-bubble mixture. However, whether the positively or negatively skewed form of $\mathcal{C}$ corresponds to some particular mixture and its dynamics, should be investigated further.

6. Summary

In most of the existing literature, the virtual mass force coefficient is defined ad-hoc or, considered empirically. Based on the virtual mass force enhanced mass fluxes for solid and fluid in mixture flow, we have analytically derived a new and full mathematical expression for the virtual mass force coefficient $\mathcal{C}$ as a function of the evolving solid fraction and the density ratio between fluid and solid particles in the mixture. As a dynamical quantity, $\mathcal{C}$ includes the dynamical and physical aspects of the mixture flow through the volume fraction ratio, and the density ratio. The new model is simple, and covers the whole domain of the dispersed solid phase, and is virtually free of fit parameters. The model is sufficiently smooth and physically well bounded with its maximum in between the dilute and dense limits of the solid fraction distribution, and evolves automatically as a function of changing solid volume fraction. This offers a much better understanding on the structure and range of the virtual mass force coefficient. Our analytical model extends the existing models and range of values of the virtual mass force by covering the whole domain of distribution of the dispersive phase, while removing the singularity or, non-physical behavior of the virtual mass force, often seen in previous models mainly in dense regime and close to the dry limit. The structure of $\mathcal{C}$ automatically removes the singularity. So, the new full analytical model for the virtual mass force can be very suitable for complex mixture flow simulations.

The form of $\mathcal{C}$ is important. We have identified the physically most relevant values for the parameters appearing in $\mathcal{C}$ that provide the well calibrated value of $\mathcal{C} = 0.5$ in literature at the vanishing solid fraction (dilute limit of the dispersed phase). As the fluid fraction vanishes, $\mathcal{C} \to 0$. This is also realistic, because as there is no fluid, no kinetic energy of the fluid needs to be induced. As the particles in the mixture become neutrally buoyant, particles and fluid tend to move together reducing the relative acceleration between them, resulting in the decreased value of $\mathcal{C}$, which is fully compatible with the physics of mixture flows. Results reveal several dynamically and mechanically important features of the new virtual mass force model in mixture flow as the solid volume fraction evolves, covering the whole domain of solid fraction. The typical mechanism of $\mathcal{C}$, first increasing to its maximum then decreasing to zero value as solid fraction increases appear here automatically from the structure of the virtual mass force induced mass fluxes, which is represented by the structure of solid to fluid fraction ratio. Another very important observation is the appearance of the density ratio in the denominator of $\mathcal{C}$. These two terms automatically remove the singularity in the new virtual mass force model.

As form of $\mathcal{C}$ is important, we have exclusively investigated on this aspect. At the vanishing solid limit, there still exists some nominal effects of enhanced mass flux, so $\mathcal{C} > 0$. But, at the vanishing fluid limit, there is almost no fluid whose kinetic energy needs to be enhanced, and thus $\mathcal{C} \to 0$. At the solid limit, the solid is so packed that this cannot mobilize the fluid to induce kinetic energy but, at the vanishing solid limit, even very small amount of particles can still induce the kinetic energy of the surrounding fluid. The numerator and denominator of $\mathcal{C}$ vary highly non-linearly and fundamentally (drastically) differently. This competition eventually controls the form of $\mathcal{C}$. Solid to fluid fraction ratio played great role in bringing $\mathcal{C}$ eventually down to zero after it attains maximum. Furthermore, the material densities, and the enhanced flux intensity fundamentally determine the form and magnitude of $\mathcal{C}$. As the density ratio increases, the virtual mass force decreases rapidly, and the peaks shift quickly towards higher values of the solid fractions. However, for the neutrally buoyant flow, the peak of the virtual mass force lies close to the middle of the particle concentration. This shows a balancing behavior of $\mathcal{C}$ both with solid fraction, and the densities. This indicates that the new virtual mass force model can potentially be applied for any type of mixture consisting of the fluid-solid and fluid-bubble, or woody debris.

Acknowledgements

We thank the reviewers, and the Editor-in-Chief, Alfredo Soldati for the very constructive comments and suggestions that substantially improved the paper. We gratefully acknowledge the financial support provided by the German Research Foundation (DFG) through the research project, PU 386/5-1: “A novel and unified solution to multi-phase mass flows”: U_MultiSol.

Supplementary material

Supplementary material associated with this article can be found, in the online version, at doi:10.1016/j.ijmultiphaseflow.2019.01.005.

References

Abbe, T.B., Montgomery, D.R., 1996. Large woody debris jams,channel hydraulics and habitat formation in large rivers. Regul. Rivers 12, 201–221.
Bagnold, R.A., 1954. Experiments on a gravity-free dispersion of large solid spheres in a newtonian fluid under shear. Proc. R. Soc. Lond. Ser. A 225, 49–63.
Biesheuvel, A., Spoelstra, S., 1989. The added mass coefficient of a dispersion of spherical gas bubbles in liquid. Int. J. Multiphase Flow 15, 911–924.
von Boetticher, A., Turowski, J.M., Mc Ardell, B.W., Rickenmann, D., Kirchner, J.W., 2016. Debrisintermixing-2.3: a finite volume solver for three-dimensional debris-flow simulations with two calibration parameters - part 1: model description. Geosci. Model Dev. 2909–2923.
Bournaski, E., 1992. Numerical simulation of unsteady multiphase pipeline flow with virtual mass effect. Int. J. Numer. Methods Eng. 34, 727–740.
Bout, B., Lombardo, L., van Westen, C.J., Jetten, V.G., 2018. Integration of two-phase solid fluid equations in a catchment model for flashfloods, debris flows and shallow slope failures. Environ. Modell. Softw. 105, 1–16. doi:10.1016/j.envsoft.2018.03.017.
Brennen, C.E., 1982. A review of added mass and fluid internal forces. Report Number: CR 82.010. Naval Civil Engineering Laboratory. Port Hueneme, California, CA 93043
Brennen, C.E., 2005. Fundamentals of Multiphase Flows. Cambridge University Press.
Cheng, L., Lahey Jr., R.T., Drew, D.A., 1983. The effect of virtual mass on the prediction of critical flow. In: Proc. 3rd CSNI Specialist Meeting,Transient Two-Phase Flow. Hemisphere, Washington, pp. 323–340. 1983
Cook, T.L., Harlow, F.H., 1984. Virtual mass in multiphase flow. Int. J. Multiphase Flow 10, 691–696.
Crosta, G.B., Negro, P.D., 2003. Observations and modelling of soil slip-debris flow initiation processes in pyroclastic deposits: the sarno 1998 event. Nat. Hazards Earth Syst. Sci. 3 (1/2), 53–69.
Dong, R.G., 1978. Effective mass and damping of submerged structures. Lawrence Livermore Laboratory. University of California Livermore, California 94550. UCRL-52342

Drew, D., 1983. Mathematical modelling of two-phase flows. Ann. Rev. Fluid Mech. 15, 261–291.
Hutter, K., Svendsen, B., Rickenmann, D., 1996. Debris flow modelling review. Continuum Mech. Thermodyn. 8, 1–35.
Ikeya, H., 1989. Debris flow and its countermeasures in japan. Bull. Int. Assoc.Eng. Geol. 40, 15–33.
Ishii, M., 1990. Two-fluid model for two-phase flow. Multiphase Sci. Technol. 5, 1–65.
Ishii, M., Hibiki, T., 2011. Thermo-Fluid Dynamics of Two-Phase Flow, 2nd ed Springer.
Ishii, M., Mishima, K., 1984. Two-fluid model and hydrodynamic constitutive relations. Nucl. Eng. Des. 82, 107–126.
Iverson, R.M., Denlinger, R.P., 2001. Flow of variably fluidized granular masses across three-dimensional terrain 1. Coulomb mixture theory. J. Geophys. Res. 106 (B1), 537–552.
Jeffrey, D.J., 1973. Conduction through a random suspension of spheres. Proc. R. Soc. Lond A335, 355–367.
Kattel, P., Kafle, J., Fischer, J.T., Mergili, M., Tuladar, B.M., Pudasaini, S.P., 2018. Interaction of two-phase debris flow with obstacles. Eng. Geol. 242, 197–217.
Kendoush, A.A., 2008. Hydrodynamic solution of the virtual mass coefficient of a vortex ring moving in a fluid. Ind. Eng. Chem. Res. 47, 1081–1084.
Khattri, K.B., Pudasaini, S.P., 2018. An extended quasi two-phase mass flow model. Int. J. Non-Linear Mech. 106, 205–222.
Kleinstreur, C.I., 2003. Two-Phase Flow: Theory and Applications. CRC Press.
Kolev, N.I., 2007. Multiphase Flow Dynamics 2: Thermal and Mechanical Interactions. Springer.
Lahey Jr., R.T., Cheng, L.Y., Drew, D.A., Flaherty, J.E., 1980. The effect of virtual mass on the numerical stability of accelerating two-phase flows. Int. J. Multiphase Flow 6, 281–294.
Lamb, H., 1952. Hydrodynamics. Cambridge University Press, Cambridge.
Lyczkowski, R.W., Gidaspow, D., Solbrig, C., Hughes, E.D., 1978. Characteristics and stability analyses of transient one-dimensional two-phase flow equations and their finite difference approximations. Nucl. Sci. Eng. 66, 378–396.
Maliska, C.R., Paladino, E.E., 2006. The role of virtual mass, lift and wall lubrication forces in accelerated bubbly flows. In: Energy: Production, Distribution and Conservation - Milan 2006, pp. 953–962.
Maxey, R.M., Riley, J.J., 1993. Equation of motion for a small sphere in a non-uniform flow. Phys. Fluids 26, 883–889.
McDougall, S., Hungr, O., 2004. A model for the analysis of rapid landslide motion across three-dimensional terrain. Can. Geotech. J. 41, 1084–1097.
Mergili, M., Emmer, A., Juricova, A., Cochachin, A., Fischer, J.T., Huggel, C., Pudasaini, S.P., 2018a. How well can we simulate complex hydro-geomorphic process chains? The 2012 multi-lake outburst flood in the santa cruz valley (Cordillera Blanca, Peru). Earth Surf. Process. Landf. 43, 1373–1389.
Mergili, M., Fischer, J.T., Krenn, J., Pudasaini, S.P., 2017. r.avaflow v1, an advanced open-source computational framework for the propagation and interaction of two-phase mass flow. Geosci. Model Dev. 10, 553–569.
Mergili, M., Frank, B., Fischer, J.T., Huggel, C., Pudasaini, S.P., 2018b. Computational experiments on the 1962 and 1970 landslide events at huascarn (Peru) with r. avaflow: Lessons learned for predictive mass flow simulations. Geomorphology 322, 15–28.
Milne-Thomson, L.M., 1968. Theoretical Hydrodynamics. MacMillan, London.
Mokeyev, Y.G., 1977. Effect of particle concentration on their drag and induced mass. Fluid. Mech. Sov. Res. 6, 161.
Mulder, T., Alexander., J., 2001. The physical character of subaqueous sedimentary density flows and their deposits. Sedimentology 48, 269–299.
Nigmatulin, R.I., 1979. Spatial averaging in the mechanics of heterogeneous and dispersed systems. Int. J. Multiphase Flow 5, 353–385.
No, H.C., Kazimi, M.S., 1981. The effect of virtual mass on the characteristics and the numerical stability in two-phase flows. Report No MIT-EL 81-023. MIT Energy Laboratory.
No, H.C., Kazimi, M.S., 1985. Effect of virtual mass on the mathematical characteristics and numerical stability of the two-fluid model. Nucl. Sci. Eng. 89, 197–206.
Prandtl, L., 1952. Essentials of fluid dynamics. Blackie & Son, Glasgow.
Pudasaini, S.P., 2011. Some exact solutions for debris and avalanche flows. Phys. Fluids 23 (4), 043301. doi:10.1063/1.3570532.
Pudasaini, S.P., 2012. A general two-phase debris flow model. J. Geophys. Res. 117 (F03010), 1–28.
Pudasaini, S.P., Hutter, K., 2007. Avalanche Dynamics: Dynamics of Rapid Flows of Dense Granular Avalanches. Springer, Berlin, New York.
Rickenmann, D., 1999. Empirical relationships for debris flows. Nat. Hadards 19, 47–77.
Rivero, M., Magnaudet, J., Fabre, J., 1991. Quelques resultants nouveaux concernat les forces exercees sur une inclusion spherique parecoulement accelere. C. R. Acad. Sci. Ser. II 312, 1499–1506.
Sangani, A.S., Zhang, D.Z., Prosperetti, A., 1991. The added mass, basset, and viscous drag coefficients in nondilute bubbly liquids undergoing small-amplitude oscillatory motion. Phys. Fluids A 3, 2955.2970.
Shields Jr., F.D., Gippe, C.J., 1995. Prediction of effects of woody debris removal on flow resistance. J. Hydraul. Eng. 121 (4), 341–354.
Simcik, M., Ruzicka, M.C., Drahos, J., 2008. Computing the added mass of dispersed particles. Chem. Eng. Sci. 63, 4580–4595.
Takahashi, T., 2007. Debris flow: mechanics, prediction and countermeasures. Taylor and Francis, London.
Thomas, N.H., Auton, T.R., Sene, K., Hunt, J.C.R., 1983. Entrapment and transport of bubbles by transient large eddies in multiphase turbulent shear flows. In: Int. Conf. on the Physical Modelling of Multi-phase Flow. Coventry, England. 19-21 April
Wallis, G.B., 1969. One-dimensional two-phase flow. McGraw-Hill, New York.
Watanabe, T., Kukita, Y., 1992. The effect of the virtual mass term on the stability of the two-fluid model against perturbations. Nucl. Eng. Des. 135, 327–340.
van Wijngaarden, L., 1976. Hodrodynamic interaction between gass bubbles in liquid. J. Fluid Mech. 77, 27–44.
Zhang, D.Z., Prosperetti, A., 1994. Averaged equations for inviscid disperse two-phase flow. J. Fluid Mech. 267, 185–219.
Zuber, N., 1964. On the dispersed two-phase flow in the laminar flow regime. Chem. Eng. Sci. 19, 897–903.